Alaska Division of Geological & Geophysical Surveys

RAW DATA FILE 2017-7

ZIRCON U-Pb AND $^{40}Ar/^{39}Ar$ RESULTS FROM DIKES COLLECTED WITHIN THE BRUIN BAY FAULT ZONE, LOWER COOK INLET

by

Robert J. Gillis, Jeff A. Benowitz, Paul B.
O'Sullivan, Paul Layer, Marwan A. Wartes

$2.00

August 2017

THIS REPORT HAS NOT BEEN REVIEWED FOR TECHNICAL CONTENT OR FOR CONFORMITY TO THE EDITORIAL STANDARDS OF DGGS

Released by
STATE OF ALASKA DEPARTMENT OF NATURAL RESOURCES
Division of Geological & Geophysical Surveys
3354 College Road
Fairbanks, Alaska 99709-3707
907-451-5010
dggs.alaska.gov

ZIRCON U-PB AND $^{40AR}/^{39AR}$ RESULTS FROM DIKES COLLECTED WITHIN THE BRUIN BAY FAULT ZONE, LOWER COOK INLET

by

Robert J. Gillis[1], Jeff A. Benowitz[2], Paul B. O'Sullivan[3,*], Paul Layer[2], Marwan A. Wartes[1]

INTRODUCTION

The Energy Resources Group from the Alaska Division of Geological & Geophysical Surveys (DGGS) has conducted topical stratigraphic, structural, and geochronologic studies along the western margin of lower Cook Inlet basin since 2009 to improve knowledge of its Mesozoic geologic framework and help spur industry interest in this under-explored region of the petroleum basin. The publicly-available geological and geochronologic data augment state- and federally-funded geologic mapping along the basin margin performed since 2013. This report presents zircon U-Pb LA-ICP-MS and $^{40}Ar/^{39}Ar$ step-heating geochronology results for one mafic and two felsic dikes in the Iliamna B-3 and C-2 quadrangles at Ursus Head and near Contact Point, lower Cook Inlet. The dikes intrude the Bruin Bay fault zone, a regional-scale system of faults that extend approximately 450 km from the upper Alaska Peninsula northeastward to upper Cook Inlet (e.g. Magoon and others, 1976), and their ages help to constrain the timing of deformation within the fault zone. The fault system is an important element of the Cook Inlet basin, as it forms the structural boundary between exhumed Mesozoic and Cenozoic magmatic arc from contemporaneous forearc basin strata along most of its length, and it likely influenced basin subsidence, sedimentation, and the growth and distribution of structural hydrocarbon traps. A mafic sill and felsic dike cut by subsidiary faults at Ursus Head returned zircon U-Pb ages of 206.9 ±0.96 (2 sigma), and 212.5 ±2.28 (2 sigma), respectively, constraining deformation associated with the fault system to younger than late Triassic. A felsic dike intruding the principal Bruin Bay fault plane near Contact Point produced biotite and plagioclase $^{40}Ar/^{39}Ar$ ages of 36.5 ±0.8 Ma and 31.5 ±0.7 Ma, respectively. The dike preserves well-developed, undeformed cooling columns oriented perpendicular to its margins, indicating that most slip along the main plane was complete by late Eocene to early Oligocene time. However, the columnar dike and the dominant fault plane are cut by one or more higher-angle faults, suggesting a change in how the fault system accommodated stress after early Oligocene time. Recent investigation of the Bruin Bay fault system by DGGS, including detailed kinematic analysis of numerous small faults within, and proximal to the structural boundary of the basin, has revealed a polyphase deformation history that occurred under separate states of stress (Betka and Gillis, 2014; 2015; 2016). A synthesis of these results and tectonic interpretation, including the new age constraints contained in this report, are published concurrently in a separate paper (Betka and others, *in press*).

[1] *Alaska Division of Geological & Geophysical Surveys, 3354 College Road, Fairbanks, AK 99709-3707; robert.gillis@alaska.gov*
[2] *Geochronology Laboratory, University of Alaska Fairbanks, Department of Geosciences, 900 Yukon Drive, P.O. Box 7555780, Fairbanks, AK 99577-5780; jbenowitz@alaska.edu*
[3] *Apatite to Zircon, Inc., 1075 Matson Rd., Viola, Idaho 83872-9709*
**Now at GeoSep Services, 1521 Pine Cone Road, Moscow, Idaho 83843; p.osullivan@geoseps.com*

The analytical data tables associated with this report are available in digital format as comma-separated value (CSV) files. See accompanying metadata file for additional details about the organization of the digital files. All files can be downloaded from the DGGS website (http://doi.org/10.14509/29750).

DOCUMENTATION OF METHODS

SAMPLE COLLECTION

Samples of igneous dikes from deformed outcrops were collected by DGGS field geologists based on their cross-cutting relationships with structural features. Sample location coordinates (in NAD27 datum) were obtained using Garmin eTrex GPS units, with typical reported accuracy of about 9 ft.

ZIRCON U-Pb SAMPLE PREPARATION

Zircon grains were isolated and prepared for Laser Ablation-Inductively Coupled Plasma-Mass Spectrometry (LA-ICP-MS) analysis using standard procedures combined with specific customized procedures described by Donelick et al. (2005). Whole rock samples were crushed using a jaw crusher with the minimum jaw separation set to 2-3 mm, sieved through 300 µm nylon mesh, and the <300 µm size fraction washed with tap water and allowed to dry at room temperature. Zircon was separated from other mineral species using a combination of lithium metatungstate (density ~2.9 g/cm^3), Frantz magnetic separator, diiodomethane (density ~3.3 g/cm^3), and hand-panning separation procedures. Epoxy wafers (~1 cm x 1 cm) containing zircon grains for LA-ICP-MS were polished manually using 3.0 µm and 0.3 µm Al_2O_3 slurries to expose internal zircon grain surfaces. The polished zircon grain surfaces were washed in 5.5 M HNO_3 for 20 s at 21° C prior to introduction into the laser system sample cell.

ZIRCON U-Pb SAMPLE ANALYSIS

LA-ICP-MS data collection was performed at the Geoanalytical Laboratory, Washington State University, Pullman, Washington, U.S.A. Individual zircon grains were targeted for data collection using a New Wave YP213 213 nm solid state laser ablation system using a 20 µm diameter laser spot size, 5 Hz laser firing rate, and ultra-high purity He as the carrier gas. Isotopic analyses of the ablated zircon material were performed using a ThermoScientific Element2 magnetic sector mass spectrometer using high purity Ar as the plasma gas. The following masses (in amu) were monitored for 0.005 s each in pulse detection mode: 202, 204, 206, 207, 208, 232, 235, and 238. At time = 0.0 s, the mass spectrometer began monitoring signal intensities; at time = 6.0 s, the laser began ablating zircon material; at time = 30.0 s, the laser was turned off and the mass spectrometer stopped monitoring signal intensities. A total of 250 data scans were collected for each zircon spot analyzed comprising: approximately 55 background scans; approximately 20 transitions scans between background and background+signal, approximately 175

background+signal scans. A scheme was developed to check whether mass 238 experienced a switch from pulse to analog mode during data collection and a correction procedure was employed to ensure the use of good quality intensity data for masses 235 and 238 when such a switch was observed.

ZIRCON U-Pb DATA REDUCTION

Previous LA-ICP-MS studies of U-Pb zircon dating used the so-called intercept method which assumes that isotopic ratio varies linearly with scan number due solely to linearly varying isotopic fractionation (Chang et al., 2006; Gehrels et al., 2008). The data modeling approach favored here was the modeling of background-corrected signal intensities for each isotope at each scan. Background intensity for each isotope was calculated using a fitted line (for decreasing background intensity) or using the arithmetic mean (for non-decreasing background intensity) at the global minimum of selected isotopes (206Pb, 232Th, and 238U) for the spot. Background+signal intensity for each isotope at each scan was calculated using the median of fitted (2nd-order polynomial) intensity values for a moving window (7 scans wide here) that includes the scan. The precision of each background-corrected signal intensity value was calculated from the precision of background intensity value and the precision of the background+signal intensity value.

Zircon U-Pb age standards used during analysis are summarized in the table below, including the 1099 ±0.6 Ma FC zircon (FC-1 of Paces and Miller, 1993) used here as the primary age standard. Isotopic data for FC were used to calculate Pb/U fractionation factors and their absolute errors for each FC data scan at each FC spot; these fractionation factors were smoothed session-wide for each data scan using the median of fitted (1st-order polynomial) fractionation factor values for a moving window (11 FC spots wide here) that includes the current FC spot and scan. Under the operating conditions of the LA-ICP-MS sessions in this study, fractionation factors were found to vary strongly with scan number, decreasing with increasing scan number (presumably due to increasing ablation pit depth and the effect this had on fractionation, (e.g., Paton et al., 2010). The zircon crystal lattice is widely known to accumulate α- radiation damage (e.g., Zhang et al., 2009 and references therein). It was assumed here that increased α-damage in a zircon leads to a decrease in the hardness of the zircon; this in turn leads to a faster rate of laser penetration into the zircon during ablation leading to dependence of isotopic fractionation on the degree of zircon lattice radiation damage. Ages calculated for all zircon age standards, when those standards were treated as unknowns, were used to construct a fractionation factor correction curve (exponential form) in terms of accumulated radiation damage. The notion of matrix-matched zircon standard and zircon unknown has been proposed largely on the basis of trace element chemistry (e.g., Black et al., 2004). In this study, time and lattice damage, parameters invisible to instruments used to characterize trace element chemistry, were introduced and applied based on measured U and Th chemistries to effectively matrix-match standard and unknown zircons.

Uranium decay constants and the $^{238}U/^{235}U$ isotopic ratio reported in Steiger and Jäger (1977) were used in this study. Errors for the isotopic ratios $^{207}Pb/^{235}Uc$ ($^{235}Uc = 137.88^{238}U$), $^{206}Pb/^{238}U$, and $^{207}Pb/^{206}Pb$ at each scan included errors from the background-corrected signal values for each isotope, the fractionation factor error, and an additional relative error term required to force 95% of the FC ages to be concordant. Ages for the ratios $^{207}Pb/^{235}Uc$, $^{206}Pb/^{238}U$, and $^{207}Pb/^{206}Pb$ were calculated for each data scan and checked for concordance; concordance here was defined as overlap of all three ages at the 1 sigma level (the use of 2 sigma level was found to skew the results to include scans with any significant common Pb). If the number of concordant data scans for a spot was greater than zero, the more precise age from the concordant-scan-weighted ratio $^{207}Pb/^{235}Uc$, $^{206}Pb/^{238}U$ or $^{207}Pb/^{206}Pb$ was chosen as the preferred age. Asymmetrical negative-direction and positive-direction age errors were calculated by subtracting and adding, respectively, the isotopic ratio errors in the appropriate age equation (Chew and Donelick, 2012).

Moving-median smoothing (MMS) is applied here to a subset (window) of *N* data points *x,y* of width *m* values of *x* to which a polynomial of order *n* is fitted. For each value of *x* at each position of the data window, a value of *y* is calculated for the fitted polynomial. The window is positioned with the right-hand boundary at the left-hand *x* value and then shifted *N-1* times until the left-hand boundary of the window is positioned at the right-hand *x* value. At each *x* position, *m* fitted values of *y* are calculated and the median of these fitted values is taken.

ZIRCON AGE STANDARDS

Standard	Standard	U-Pb age (± 2σ)	Reference
FC	Duluth complex	1,099.0 ± 0.6 Ma	Paces and Miller, 1993
F5	Duluth complex	1,099.0 ± 0.6 Ma (assumed equal to FC-1)	Paces and Miller, 1993
IF	Fish Canyon Tuff	28.201 ± 0.012 Ma	Lanphere and Baadsraard, 2001; Kuiper and others, 2008
MD	Mount Dromedary	99.12 ± 0.14 Ma	Renne and others, 1998
PX	Peixe	563.5 ± 1.6 Ma	Gehrels and others, 2008
R3	Braintree complex	418.9 ± 0.4 Ma	Black and others, 2004
T2	Temora 2, Middledale gabbroic diorite	416.78 ± 0.33 Ma	Black and others, 2004
TR	Tardree Rhyolite	61.23 ± 0.11 Ma	Dave Chew, pers. commun.

ZIRCON U-Pb RESULTS

The accompanying tables provide a summary of all the U-Pb results, sample locations, experiment results for individual samples. All ages quoted to the ±2 sigma level. Kernel density

estimates were made using DensityPlotter v. 7.3 (Vermeesch, 2012), and Concordia and weighted mean plots were constructed with Isoplot v. 4.15 (Ludwig, 2003).

$^{40}Ar/^{39}Ar$ SAMPLE PREPARATION

One rock sample was submitted to the UAF Geochronology Laboratory for $^{40}Ar/^{39}Ar$ analysis, where it was crushed, sieved, washed, and hand-picked for phenocryst-free rock chips (1,000–500 micron size fraction) and biotite and feldspar mineral phases (1,000–150 microns). The monitor mineral MMhb-1 (Samson and Alexander, 1987) with an age of 523.5 Ma (Renne and others, 1994) was used to monitor neutron flux (and calculate the irradiation parameter, J). The crystals and standards were wrapped in aluminum foil and loaded into aluminum cans of 2.5 cm diameter and 6 cm height. The crystals were irradiated in position 5c of the uranium-enriched research reactor of McMaster University in Hamilton, Ontario, Canada, for 20 megawatt-hours.

$^{40}Ar/^{39}Ar$ SAMPLE ANALYSIS

Upon their return from the reactor, the crystals and monitors were loaded into 2-mm-diameter holes in a cop- per tray, which was then loaded into an ultra-high-vacuum extraction line. The monitors were fused, and crystals heated, using a 6-watt argon-ion laser following the technique described in York and others (1981), Layer and others (1987), and Benowitz and others, (2014). Argon purification was achieved using a liquid nitro- gen cold trap and an SAES Zr-Al getter at 400°C. The crystals were analyzed in a VG-3600 mass spectrometer at the UAF Geophysical Institute. The argon isotopes measured were corrected for system blank and mass discrimination, as well as calcium, potassium, and chlorine interference reactions following procedures outlined in McDougall and Harrison (1999). Typical full-system 8 min laser blank values (in moles) were generally 2×10^{-16} mol ^{40}Ar, 3×10^{-18} mol ^{39}Ar, 9×10^{-18} mol ^{38}Ar and 2×10^{-18} mol ^{36}Ar, which are 10–50 times smaller than the sample/standard volume fractions. Correction factors for nucleogenic interferences during irradiation were determined from irradiated CaF_2 and K_2SO_4 as follows: $(^{39}Ar/^{37}Ar)Ca = 7.06 \times 10^{-4}$, $(^{36}Ar/^{37}Ar)Ca = 2.79 \times 10^{-4}$ and $(^{40}Ar/^{39}Ar)K = 0.0297$. Mass discrimination was monitored by running calibrated air shots. The mass discrimination during these experiments was 1.3 percent per mass unit. Throughout the data collection process, calibration measurements were made on a weekly–monthly basis to check for changes in mass discrimination, with no significant variation seen during these intervals.

$^{40}Ar/^{39}Ar$ RESULTS

The accompanying tables provide a summary of all the $^{40}Ar/^{39}Ar$ calculations and the experimental results. Summary ages are quoted to the ±1 sigma level and calculated using the constants of Renne and others (2010). The integrated age is the age given by the total gas measured and is equivalent to a potassium-argon (K-Ar) age. The spectrum provides a plateau age if three or more consecutive gas fractions represent at least 50 percent of the total gas release and are within two standard deviations of each other (Mean Square

Weighted Deviation [MSWD] less than 2.5). $^{40}Ar/^{39}Ar$ plots are provided by the University of Alaska geochronology laboratory.

DISCUSSION

Below we provide a brief discussion of the results of each age analysis from the Ursus Head and the Contact Point areas.

Sills and dikes exposed in a coastal exposure at Ursus Head are deformed within the Bruin Bay fault zone (Betka and Gillis, 2015; Gillis and others, 2011). Common dikes intruding late Triassic Kamishak Formation strata composing the hanging-wall of the Bruin Bay fault (Detterman and Reed, 1980) are cut by numerous small-scale, low-angle, bedding-parallel, and high angle contractional faults (Betka and others, *in press*). Sample 09MAW006A collected from one of many dikes deformed in the fault zone produced a uni-modal distribution of zircon ages of with a weighted mean of 206.92 ±0.96 (2σ, n=47) and an MSWD of 1.1 (Figure. 1). Sample 09BG020C collected from a sill of more mafic composition yielded few zircons and produced only eight ages with a weighted mean of 212.49 ±2.28 (2σ) and an MSWD of 3.42 (Figure. 2). The dikes and sills likely intruded very early post-deposition, based on the abundance of late Triassic *Monotis* fossils in the country rock observed during this field study and the middle to late Norian fossil assemblage (approximately 208-204 Ma) reported within nearby Kamishak strata in Ursus Cove by Detterman and Reed (1980). The relationship of these Triassic igneous rocks to Talkeetna arc magmatism is uncertain. Kamishak Formation strata are intruded by the Talkeetna arc batholith and depositionally overlain by related arc volcanics within 5 km of Ursus Head (Detterman and Reed, 1980). Available zircon U-Pb analyses of Talkeetna arc intrusives in lower Cook Inlet produced only Jurassic ages ranging from 183.5-164.1 Ma (Rioux and others, 2010). The oldest published age assigned to the Talkeetna volcanic arc edifice in this region is 207 ±5 Ma from a volcanic breccia associated with fossiliferous limestone located along strike approximately 80 km to the northeast between the Johnson River and Tuxedni Bay (Amato and others, 2007). The age and associated facies at the Johnson River locality suggest it may be correlative with the Kamishak Formation at Ursus Head, rather than the Talkeetna Formation. The tectonic affinity of these Upper Triassic igneous rocks remains unclear and it's possible they do *not* represent an early record of Talkeetna arc magmatism in this area.

Roughly 7 km southwest of Contact Point, Jurassic rocks forming a high coastal bluff are cut by the principal plane of the Bruin Bay fault system, where the fault contact between hanging-wall Talkeetna Formation arc volcanics and footwall Naknek Formation forearc basin strata are intruded by two distinct dikes of felsic to intermediate composition (Gillis and others, 2013). The lower dike is approximately 2-3 m thick, porphyritic with common hornblende and biotite phenocrysts up to 4 mm long, and weathers light gray. The upper dike from which sample 12BG109A was collected is approximately 3-4 m thick, porphyritic with common plagioclase and biotite phenocrysts up to 4 mm and 2.5 mm long, respectively, and weathers pale pink. A

striking feature of the upper dike is its well-developed, 15-30 cm wide and up to 3 m tall cooling columns preserved orthogonally to the fault contact. The contact between the dike and the hanging-wall Talkeetna Formation is intrusive and marked by a 2-5cm wide baked zone. The dike over much of its exposed length is only moderately to lightly fractured, indicating little movement on the principal plane after emplacement, but is offset by a steeper fault hindward of the main Bruin Bay fault exposure (Betka and others, *in press*). An analysis of a biotite fraction yielded an integrated age of 35.5 ±0.9 Ma, a plateau age of 36.5 ±0.8 Ma, and the isochron age of 36.3 ±1.1 Ma, that are identical within analytical error (Figure 3). The plateau age of 36.5 ±0.8 Ma is preferred because of the higher precision over the integrated and isochron age and because of the large error on the regression to initial ^{40}Ar. An analysis of a plagioclase fraction yielded an integrated age of 31.6 ±0.8 Ma, a plateau age of 31.5 ±0.7 Ma, and the isochron age of 30.8 ±0.7 Ma, that are identical within analytical error (Figure 3). The isochron age of 30.8 ±0.7 Ma is preferred because of the higher precision over the integrated age and because the regression to initial ^{40}Ar indicates slight excess ^{40}Ar.

Assuming relatively rapid cooling from emplacement temperature based on the presence of well-formed cooling columns, the biotite age is interpreted to approximate the age of injection. However, the 5.7 Ma younger plagioclase cooling age requires significantly slower cooling at 9 ˚C/Ma, which is interpreted to reflect hanging-wall denudation, rather than steady-state post-emplacement cooling (Betka and others, *in press*). With the exception of few, relatively thin dikes (e.g. Rosenthal and others, 2017; Betka and others, *in press*), middle to late Eocene plutonic and volcanic arc rocks are rare along the Bruin Bay fault system trend in lower Cook Inlet. Yet approximately 30 km to the northwest near Iliamna Lake, middle to late Eocene volcanics are common, and partially delineate an approximately 800 km-long swath of volcanic arc strata discontinuously exposed from near the southern tip of the Alaska Peninsula to the Capps Glacier area in upper Cook Inlet to the northeast (Detterman and Reed, 1980; Wilson, 1985; Wilson and others, 1999; Todd and others, 2014; Gillis and others, in preparation). The two occurrences of Eocene volcanics recently recognized intruding the Bruin Bay fault zone near Contact Point and at Ursus Head (Betka and others, *in press*; this report) might suggest that the arcward-dipping structural boundary between the Eocene arc and forearc basin served as a conduit for transporting minor arc melts at depth to a more forearc position.

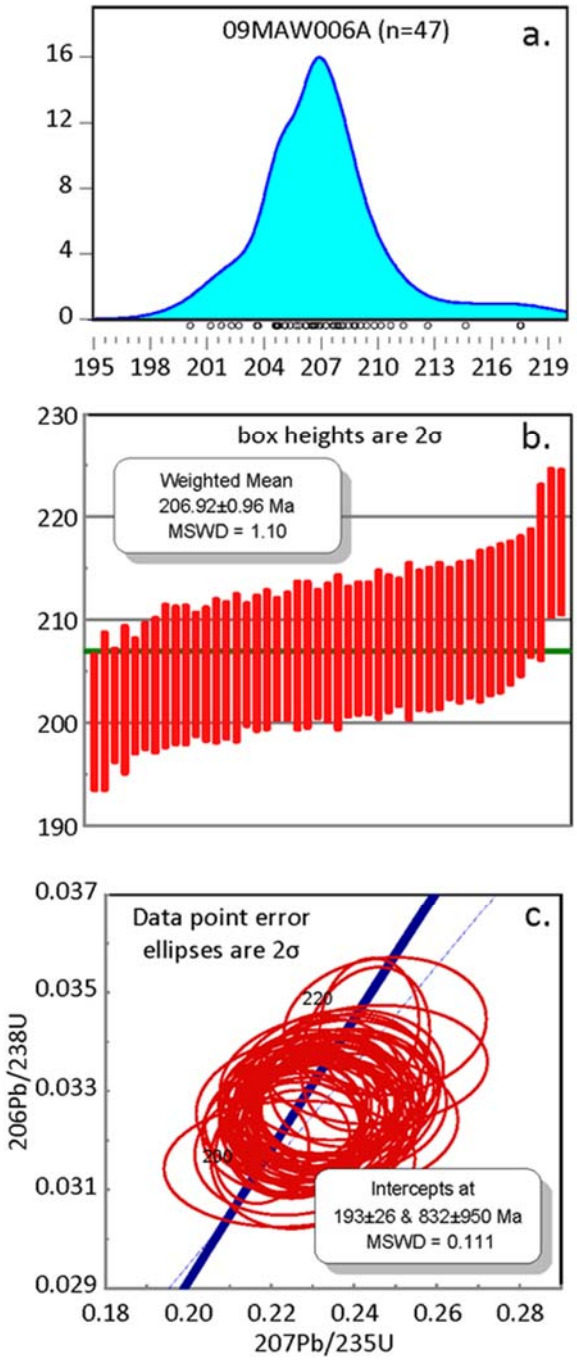

Figure 1. U-Pb plots for sample 09MAW006A. a. Kernel density estimate and distribution of individual grain ages (small open circles). b. Weighted mean diagram of all sample grain ages. Width of red bars reflect grain age errors at the 2 sigma level. c. Concordia diagram demonstrating a closed U-Pb system (within 2 sigma analytical error).

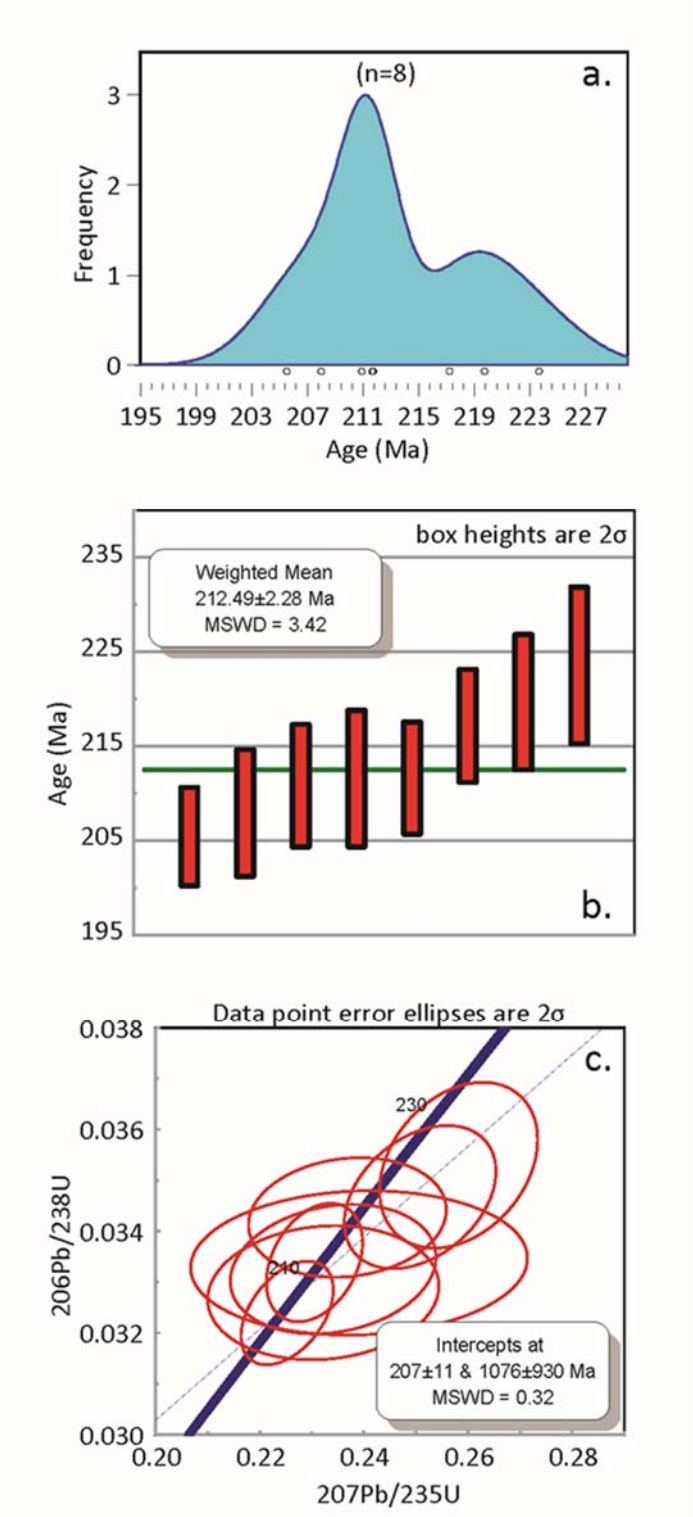

Figure 2. U-Pb plots for sample 09BG020C. a. Kernel density estimate and distribution of individual grain ages (small open circles). b. Weighted mean diagram of all sample grain ages. Width of red bars reflect grain age errors at the 2 sigma level. c. Concordia diagram demonstrating a closed U-Pb system (within 2 sigma analytical error).

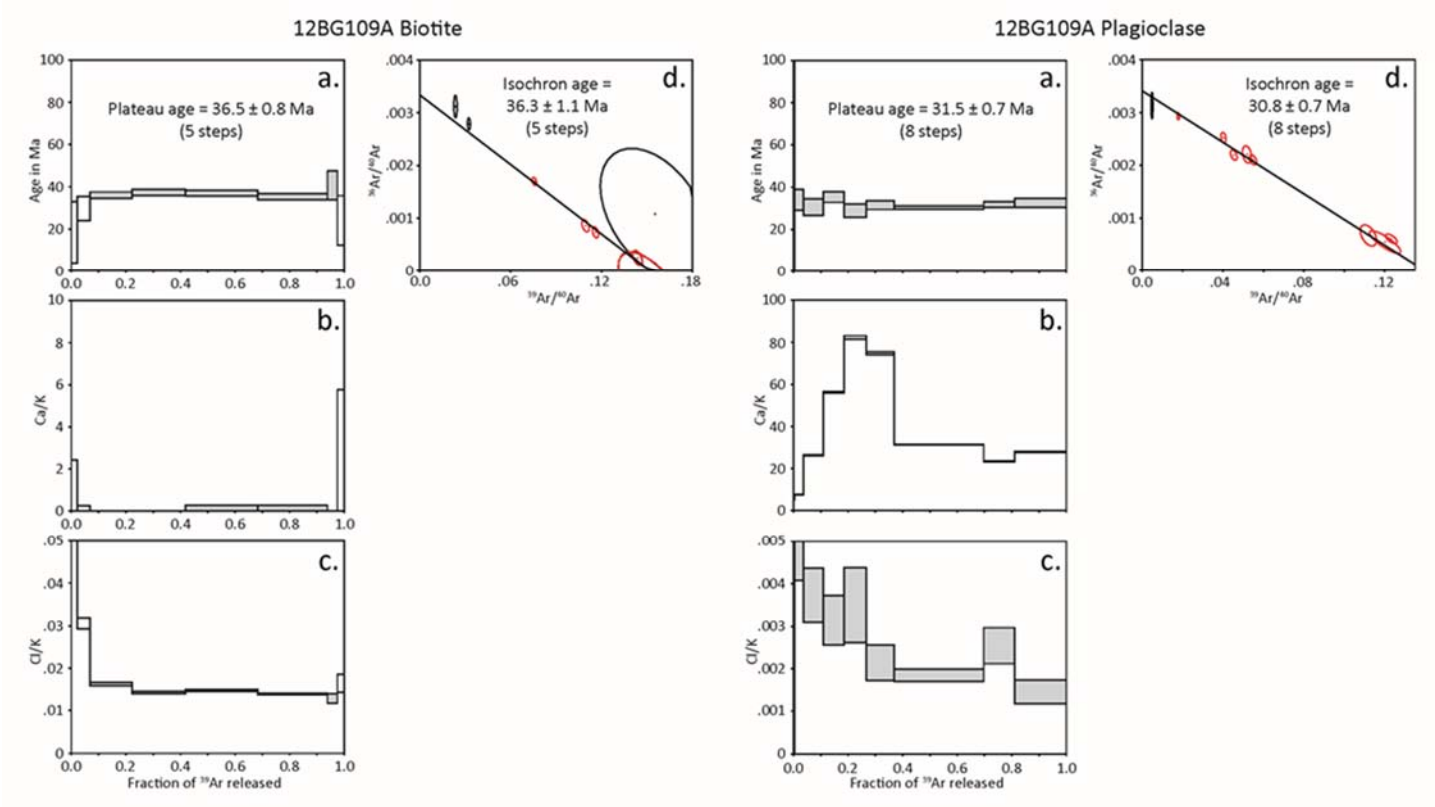

Figure 3. Biotite and plagioclase $^{40}Ar/^{39}Ar$ plots for sample 12BG109A. a. age in Ma versus fraction of ^{39}Ar released as a function of 8 heating steps. b. Calcium/potassium ratio versus fraction of ^{39}Ar released as a function of 8 heating steps. c. Chlorine/potassium ratio versus fraction of ^{39}Ar released as a function of 8 heating steps. d. Regressed inverse isochron comparing atmospheric (^{36}Ar) versus radiogenic (^{39}Ar) argon for each heating step.

ACKNOWLEDGEMENTS

Lower Cook Inlet field studies in 2009 and 2012 were funded by the State of Alaska. We appreciate Pathfinder Aviation and pilot Merlin (Spanky) Handley for the helicopter support, Jack Barber at Alaska Air Taxi and Jose de Creeft at Northwind Aviation for charter fixed wing services, James and Shelia Isaak at Alaska Homestead Lodge, and Ray and Linda Williams at their lodge at Pile Bay for accommodations while performing field work. Lastly, we wish to thank Bob Swenson for drawing our attention to these spectacular outcrops, and who spent many hours pondering their significance.

REFERENCES

Amato, J. M., Rioux, M.E., Kelemen, P.B., Gehrels, G.E., Clift, P.D., Pavlis, T.L., and Draut, A.E., 2007, U-Pb geochronology of volcanic rocks from the Jurassic Talkeetna Formation and detrital zircons from prearc and postarc sequences: Implications for the age of magmatism and inheritance in the Talkeetna arc, in Tectonic Growth of a Collisional Continental Margin, *in* Crustal Evolution of Southern Alaska, Ridgway et al. (ed), Spec. Pap. Geol. Soc. Am., 431, 253–271, doi:10.1130/2007.2431(11).

Benowitz, J.A., Layer, P.W., and Vanlaningham, S., 2014, Persistent long-term (c. 24 Ma) exhumation in the eastern Alaska Range constrained by stacked thermochronology: London, Geological Society of London, Special Publication 378, no. 1, p. 225–243.

Black, L.P., Kamo, S.L., Allen, C.M., Davis, D.W., Aleinikoff, J.N., Valley, J.W., Mundil, Roland, Campbell, I.H., Korsch, R.J., Williams, I.S., and Foudoulis, Chris, 2004, Improved $^{206}Pb/^{238}U$ microprobe geochronology by the monitoring of trace-element-related matrix effect—SHRIMP, ID-TIMS, ELA-ICP-MS, and oxygen isotope documentation for a series of zircon standards: Chemical Geology, v. 205, p. 15–140.

Betka, P.M., and Gillis, R.J., 2014, Preliminary characterization of brittle deformation on the Iniskin Peninsula: Implications for the kinematic history of the Bruin Bay fault system, lower Cook Inlet, Alaska: Alaska Division of Geological & Geophysical Surveys Preliminary Interpretive Report 2014-5, 14 p. http://doi.org/10.14509/29130

Betka, P.M., and Gillis, R.J., 2015, The superposition of strike-slip and reverse-slip faults in the Bruin Bay fault system, Ursus Head, lower Cook Inlet, in Wartes, M.A., ed., Energy-related studies during the 2014 field season, western Cook Inlet, Alaska: Alaska Division of Geological & Geophysical Surveys Preliminary Interpretive Report 2015-5-2, p. 5-8. http://doi.org/10.14509/29457

Betka, P.M., and Gillis, R.J., 2016, Observations on the Bruin Bay fault system between Chinitna and Tuxedni bays, Cook Inlet, Alaska, in Herriott, T.M., ed., Petroleum-related geologic studies in lower Cook Inlet during 2015, Iniskin-Tuxedni region, south-central Alaska: Alaska Division of Geological & Geophysical Surveys Preliminary Interpretive Report 2016-1-10, p. 73-78. http://doi.org/10.14509/29544

Betka, P.M., Gillis, R.J., and Benowitz, J.A., *in press*, Cenozoic sinistral-transpression and polyphase-slip within the Bruin Bay fault system; Iniskin-Tuxedni region, Cook Inlet, Alaska: Geosphere, v. xx, p. xxx-xxx

Chang, Zhaoshan, Vervoort, J.D., McClelland, W.C., and Knaack, Charles, 2006, U-Pb dating of zircon by LA-ICP-MS: Geochemistry, Geophysics, Geosystems, American Geophysical Union, v. 7, no. 5, 14 p., doi:10.1029/2005GC001100.

Chew, D.M., and Donelick, R.A., 2012, Combined apatite fission track and U-Pb dating by LA-ICP-MS and its application in apatite provenance analysis: Mineralogical Association of Canada Short Course, v. 42, p. 219–247.

Detterman, R.L., and Reed, B.L., 1980, Stratigraphy, structure, and economic geology of the Iliamna Quadrangle, Alaska: U.S. Geological Survey Bulletin 1368-B, p. B1-B86, 1 sheet, scale 1:250,000.

Donelick, R.A, O'Sullivan, P.B., and Ketcham, R.A., 2005, Apatite fission-track analysis: Reviews in Mineralogy and Geochemistry, Mineralogical Society of America, v. 58, p. 49–94.

Gehrels, G.E., Valencia, V.A., and Ruiz, J., 2008, Enhanced precision, accuracy, efficiency, and spatial resolution of U-Pb ages by laser ablation–multicollector–inductively coupled plasma–mass spectrometry: Geochemistry Geophysics Geosystems, American Geophysical Union, v. 9, 13 p.

Gillis, R.J., Wartes, M.A., and O'Sullivan, P.B., 2011, Preliminary findings from reconnaissance structural studies along the Bruin Bay fault system and adjacent areas, south-central Alaska: AAPG Pacific Section Meeting, Anchorage, Alaska, May 10, 2011: Alaska Division of Geological & Geophysical Surveys, 1 sheet. http://doi.org/10.14509/23403

Gillis, R.J., Swenson, R.F., Wartes, M.A., and Frohman, R.A., 2013, Reconnaissance investigations of the Bruin Bay fault system along the western margin of lower Cook Inlet and upper Alaska Peninsula, in Gillis, R.J., ed., Overview of 2012 field studies: Upper Alaska Peninsula and west side of lower Cook Inlet, Alaska: Alaska Division of Geological & Geophysical Surveys Preliminary Interpretive Report 2013-1G, p. 33-37. http://doi.org/10.14509/24850

Gillis, R.J., LePain, D.L., Benowitz, J.A., O'Sullivan, P.B., Layer, P.W., and Drake, J., *in preparation*, $^{40}Ar/^{39}Ar$ and U-Pb geochronologic age constraints for Kenai Group strata and late Cretaceous to Paleocene volcanic and intrusive rocks, south-central Tyonek Quadrangle, northwestern Cook Inlet region, Alaska, Division of Geological & Geophysical Surveys Report of Investigation

Kuiper, K.F., Deino, A., Hilgen, P.J., Krijgsman, W., Renne, P.R., and Wijbrans, J.R., 2008, Synchronizing rock clocks of Earth history: Science, v. 320, p. 500–504.

Lanphere, M.A., and Baadsraard, H., 2001, Precise K-Ar, $^{40}Ar/^{39}Ar$, Rb-Sr and U-Pb mineral ages from the 27.5 Ma Fish Canyon Tuff reference standard: Chemical Geology, v. 175, p. 653–671.

Layer, P.W., Hall, C.M., and York, Derek, 1987, The derivation of $^{40}Ar/^{39}Ar$ age spectra of single grains of horn- blende and biotite by laser step-heating: Geophysical Research Letters, v. 14, no. 7, p. 757–760.

Ludwig, K.R., 2003, User's manual for Isoplot 3.00: A geochronological toolkit for Microsoft Excel, no. 4, Berkeley Geochronology Center, Berkeley.

Magoon, L.B., Adkison, W.L., and Egbert, R.M. (1976). Map showing geology, wildcat wells, Tertiary plant fossil localities, K-Ar age dates, and petroleum operations, Cook Inlet area, Alaska: U.S. Geological Survey Miscellaneous Investigations Series Map 1019, 3 sheets, scale 1:250,000.

McDougall, Ian, and Harrison, T.M., 1999, Geochronology and thermochronology by the $^{40}Ar/^{39}Ar$ method, 2nd edition: New York, Oxford University Press, 269 p.

Paces, J.B., and Miller, J.D., 1993, Precise U-Pb ages of Duluth Complex and related mafic intrusions, northeastern Minnesota—Geochronological insights to physical, petrogenic, paleomagnetic, and tectonomagmatic processes associated with the 1.1 Ga Midcontinent Rift System: Journal of Geophysical Research, v. 98, no. B8, p. 13,997–14,013.

Paton, C., Woodhead, J.D., Hellstrom, J.C., Hergt, J.M., Greig, A., and Maas, R., 2010, Improved laser ablation U-Pb zircon geochronology through robust downhole fractionation correction: Geochemistry, Geophysics, Geosystems, v. 11, no. Q0AA06, doi:10.1029/2009GC002618.

Renne, P.R., Mundil, Roland, Balco, Greg, Min, Kyoungwon, and Ludwig, K.R., 2010, Joint determination of ^{40}K decay constants and $^{40}Ar/^{40}K$ for the Fish Canyon sanidine standard, and improved accuracy for $^{40}Ar/^{39}Ar$ geochronology: Geochimica et Cosmochimica Acta, v. 74, no. 18, p. 5,349–5,367.

Renne, P.R., Deino, A.L., Walter, R.C., Turrin, B.D., Swisher, C.C., Becker, T.A., Curtis, G.H., Sharp, W.D., and Jaouni, A.R., 1994, Intercalibration of astronomical and radioisotopic time: Geology, v. 22, no. 9, p. 783–786. doi:10.1130/0091-7613(1994)022<0783:IOAART>2.3.CO;2

Renne, P.R., Swisher, C.C., Deino, A.L., Karner, D.B., Owens, T.L., and DePaolo, D.J., 1998, Intercalibration of standards, absolute ages and uncertainties in $^{40}Ar/^{39}Ar$ dating: Chemical Geology, v. 45, p. 117–152.

Rioux, M., Mattison, J., Hacker, B., Kelelman, P., Blusztajn, J., Hanghoj, K., and Gehrels, G., 2010, Intermediate to felsic middle crust in the accreted Talkeetna arc, the Alaska Peninsula and Kodiak Island, Alaska: An analog for low-velocity middle crust in modern arcs, Tectonics, v. 29, TC3001, doi:10.1029/2009TC002541

Samson, S.D., and Alexander, E.C., 1987, Calibration of the interlaboratory $^{40}Ar/^{39}Ar$ dating standard, MMhb-1: Chemical Geolology, Isotope Geoscience Section, v. 66, no. 1-2, p. 27–34.

Steiger, R.H., and Jäger, E., 1977, Subcommission on geochronology—Convention on the use of decay constants in geo- and cosmochronology: Earth and Planetary Science Letters, v. 36, p. 369–371.

Todd, E., Jones, J.V. III, Karl, S., Ayuso, R.A., Bradley, D.C., Box, S.E., and Haeusler, P.J., 2014, Magmatic responses to Late Cretaceous through Oligocene tectonic evolution of the western Alaska Range, V32B-06 presented at 2014 Fall Meeting, AGU, San Francisco, Calif., 15-19 Dec.

Vermeesch, P., 2012. On the visualisation of detrital age distributions. Chemical Geology, v.312-313, 190-194, doi: 10.1016/j.chemgeo.2012.04.021 0

Wilson, F.H., 1985, The Meshik Arc - an eocene to earliest miocene magmatic arc on the Alaska Peninsula: Alaska Division of Geological & Geophysical Surveys Professional Report 88, 14 p. http://doi.org/10.14509/2269

Wilson, F.H., Detterman, R.L., and DuBois, G.D., 1999, Digital data for the geologic framework of the Alaska Peninsula, Southwest Alaska, and the Alaska Peninsula terrane: U.S. Geological Survey Open-File Report 99-317, 41 p., 1 sheet.

York, Derek, Hall, C.M., Yanase, Yotaro, Hanes, J.A., and Kenyon, W.J., 1981 $^{40}Ar/^{39}Ar$ dating of terrestrial minerals with a continuous laser: Geophysical Research Letters, v. 8, no. 11, p. 1,136–1,138.

Zhang, M., Ewing, R.C., Boatner, L.A., Salje, E.K.H., Weber, W.J., Daniel, P., Zhang, Y., and Farnan, I., 2009, Pb^{*} irradiation of synthetic zircon ($ZrSiO_4$); Infrared spectroscopic study—Reply: American Mineralogist, v. 94, p. 856–858.